ACS APPLIED MATERIALS & INTERFACES

Research Article

www.acsami.org

Versatile Wafer-Scale Technique for the Formation of Ultrasmooth and Thickness-Controlled Graphene Oxide Films Based on Very Large Flakes

Joël Azevedo,[†] Stéphane Campidelli,[*,†] Delong He,[‡] Renaud Cornut,[†] Michael Bertucchi,[†] Sébastien Sorgues,[§] Jean-Jacques Benattar,[‡] Christophe Colbeau-Justin,[§] and Vincent Derycke[*,†]

[†]CEA Saclay, IRAMIS, NIMBE (UMR 3685), LICSEN, F-91191 Gif sur Yvette, France

[‡]CEA Saclay, IRAMIS, SPEC, F-91191 Gif sur Yvette, France

[§]University Paris-Sud and CNRS, Laboratoire de Chimie Physique, UMR 8000, F-91405 Orsay, France

Supporting Information

ABSTRACT: We present a new strategy to form thickness-adjusted and ultrasmooth films of very large and unwrinkled graphene oxide (GO) flakes through the transfer of both hemispherical and vertical water films stabilized by surfactants. With its versatility in terms of substrate type (including flexible organic substrates) and in terms of flake density (from isolated flakes to continuous and multilayer films), this wafer-scale assembly technique is adapted to a broad range of experiments involving GO and rGO (reduced graphene oxide). We illustrate its use through the evaluation of transparent rGO electrodes.

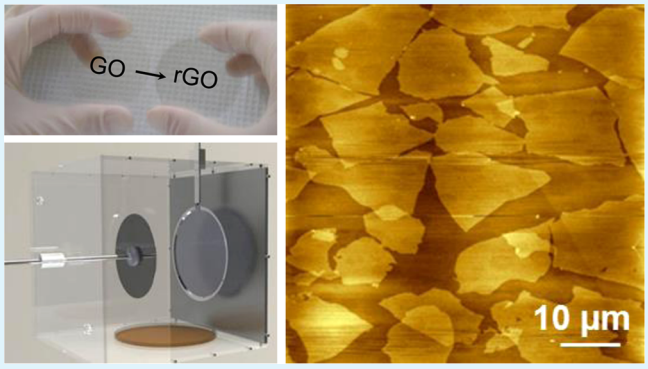

KEYWORDS: *graphene oxide, transfer method, ultrathin films, transparent electrodes, large flakes, wafer scale*

1. INTRODUCTION

The importance of graphene and analogues in future applications ranging from composite materials to electronics, optoelectronics, and energy sources is well established.[1−3] However, the large-scale development of viable applications for graphene is conditioned by the availability of material sources that meet stringent quality and cost requirements. Two classes of options for such development at the material level are gaining momentum because of sizable advantages: the chemical vapor deposition (CVD) growth associated with a transfer process on the one hand[4] and the liquid route on the other hand. CVD-grown graphene displays very high carrier mobility. However, because of cost and complexity limitations, it may be mostly appropriate for very high added value markets such as high-frequency electronics.[5,6] Conversely, the liquid route gathers highly valuable specificities that make it attractive for large-area applications in particular in printable electronics and optoelectronics or energy-related devices and systems. Direct liquid phase exfoliation of graphite[7−11] through harsh sonication still produces small graphene flakes (typically in the 0.05−0.4 μm^2 range for pure graphene monolayers) with limited control of the thickness distributions (except for flakes sorted by density gradient ultracentrifugation[7]) and limited yield. An alternative route is based on the oxidation of graphite followed by the exfoliation of graphite oxide in aqueous or polar organic solvents.[12,13] This method is considered as one of the most promising ways to obtain purely monolayered graphene oxide (GO) flakes that can then be chemically or thermally reduced to obtain reduced graphene oxide (rGO).[14−16] Besides, this approach is the only one able to yield, from graphite, stable solutions of very large size sheets (up to 7000 μm^2)[15−17] whose benefits are recognized, in particular for rGO-based electrodes.[16,18]

Such a solution-based approach holds great promises because the dispersed material can be assembled in thin films on almost any type of surface. One of the crucial challenges in the field is to propose and optimize simple, scalable, and reproducible methods to precisely control the deposition of graphene oxide sheets in single and multilayer films with well-controlled parameters (thickness, homogeneity, roughness).[19,20] Several deposition techniques proved very efficient for the assembly of small-size GO sheets.[21−23] However, the assembly of extremely large GO sheets imposes new constraints on the deposition methods. Intuitively, the smaller the flakes are, the easier is their deposition in an unfolded and unwrinkled manner. However, beyond the size criterion, the difference also extends to the chemical properties of each type of flakes: small GO sheets are hydrophilic while larger ones are amphiphilic.

Received: June 22, 2015
Accepted: September 8, 2015
Published: September 8, 2015

DOI: 10.1021/acsami.5b05540
ACS Appl. Mater. Interfaces 2015, 7, 21270−21277

Among the various traditional techniques used to form thin GO films,[21−30] the Langmuir−Blodgett is the most efficient in assembling large and unfolded sheets, but limitations still remain. In particular, the film roughness experiences a significant deterioration as soon as the deposition exceeds a single layer.[15,21] Thus, the development of new techniques that lead to optimized films over large areas is still a pressing issue.

We report here a new strategy to form thickness-adjusted and ultrasmooth films of very large GO flakes. We start by extending to the case of very large (100−400 μm^2) flakes, a deposition method that we recently developed for small (1 μm^2) flakes (the so-called bubble deposition method (BDM)[23]) and which is based on the transfer of hemispherical surfactant-stabilized water films incorporating GO. We then overcome the main limitations of this initial geometry (in particular in terms of sample size) by substituting the hemispherical film shape with large and vertical water films. Such decisive improvement makes the method very efficient for the wafer-scale transfer of high-quality GO films. After chemical reduction and thermal annealing, GO films are converted into transparent electrodes exhibiting performances among the best reported to date for rGO films in terms of transmittance and sheet resistance.

2. RESULTS AND DISCUSSION

2.1. Transfer of Hemispherical Films. Recently, we developed a generic deposition method for the assembly of various types of nano-objects on the basis of their confinement in the water core of hemispherical surfactant-stabilized films. This bubble deposition method notably proved very powerful for the formation of dense films of nanowires,[31] proteins,[32] nanotubes,[33] and small GO flakes.[23] Figure 1 illustrates this method and its evolution to the case of large GO flakes (note that the size ranges of GO flakes were named using the terminology introduced in ref 14). The procedure involves the following steps (see Experimental Section for details and Figure S1 for a schematic of the deposition chamber and protocol): first, a small volume of a solution of the desired nano-objects in water/sodium dodecylbenzene-sulfonate is used to form a bubble-shaped film within a closed and humidity-saturated glass chamber. In the case of small GO flakes, the nano-objects gather between two surfactant monolayers assembled at the air/water interfaces. The drainage of the water core then leads to a decrease of the surfactant-stabilized water film thickness and therefore to an increase of the confinement of the nano-objects, enabling a preorganization. At the desired bubble-wall thickness (precisely controllable through its effect on the bubble color change), a substrate is approached to transfer this surfactant-stabilized water film. After bubble bursting, the remaining water quickly evaporates, and the surfactant is then eliminated by first drying the sample on a hot plate (50 °C) and then by rinsing with water and ethanol. The process and a corresponding atomic force microscopy (AFM) image of the GO film are presented in Figure 1b. This deposition method is highly efficient when dealing with small hydrophilic GO sheets. However, the controlled assembly of very large GO flakes (with areas more than 100 times larger) is obviously a different challenge in particular because of their amphiphilic properties.[34,35]

Large GO flakes were synthesized by a modified Hummers' method followed by mild exfoliation (see Experimental Section). Because of their amphiphilic character, these large flakes preferentially assemble at the air/water interface and

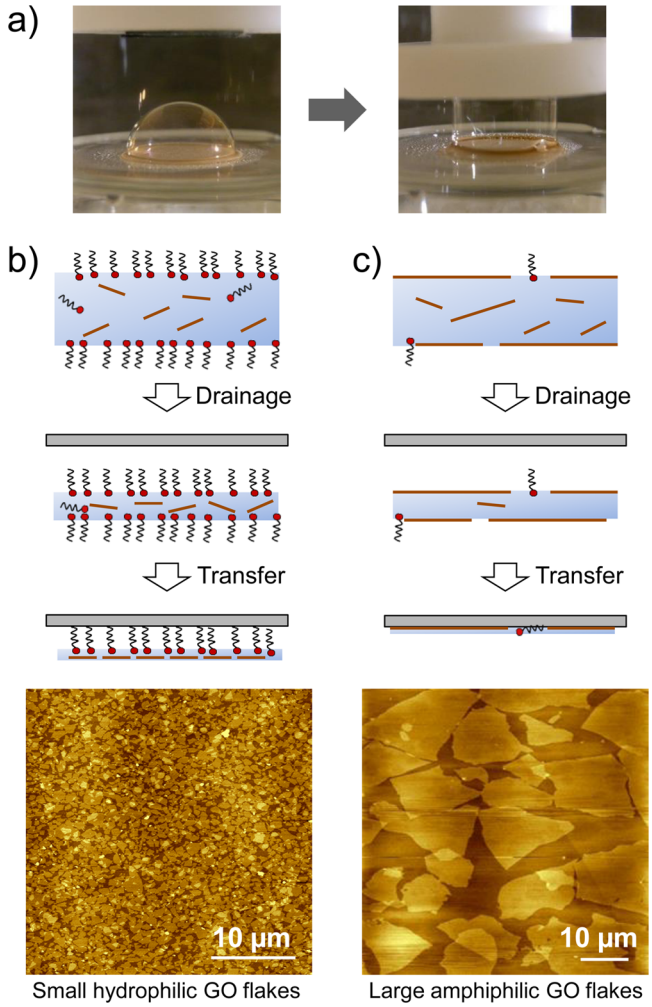

Figure 1. Principle of graphene oxide deposition. (a) Photographs of the transfer step from a hemispherical bubble (diameter 1.2 cm). Before bursting, the surfactant-stabilized water film adopts a cylindrical shape. (b) Schematic representation of the top part of the bubble wall in the case of small GO flakes (schematically represented as brown bars in the water core of the bubble wall; GO flakes and surfactant molecules are not represented at the same scale for clarity) and AFM image of the deposited film. (c) Same representation in the case of large amphiphilic GO flakes. Large GO flakes being principally at the water/air interface, they lie directly on the substrate after transfer, without an intercalated surfactant layer.

participate in the stabilization of the water films.[21] Surfactant is, however, still needed to improve the stability of the bubble wall. Figure 1c illustrates the main differences with the case of small flakes and confirms all the benefits of this approach for large and flat sheet deposition: large amphiphilic GO flakes being principally at the water/air interface, they lie directly on the substrate after transfer, without an intercalated surfactant or water layer. Hypothetic traces of remaining surfactant would be easily identified by AFM as shown in Figure S2 displaying the situation between the drying and rinsing steps.

Before transfer, the water drainage is used to control the density of the deposited objects. This drainage parameter being finely adjustable, it makes the method particularly powerful for substrate coating and allows tuning the density of flakes from isolated objects (Figure 2a) to close-packed arrangements (Figures 1c and 2b). Importantly, compared with traditional solution deposition methods, the high efficiency of this

DOI: 10.1021/acsami.5b05540
ACS Appl. Mater. Interfaces 2015, 7, 21270−21277

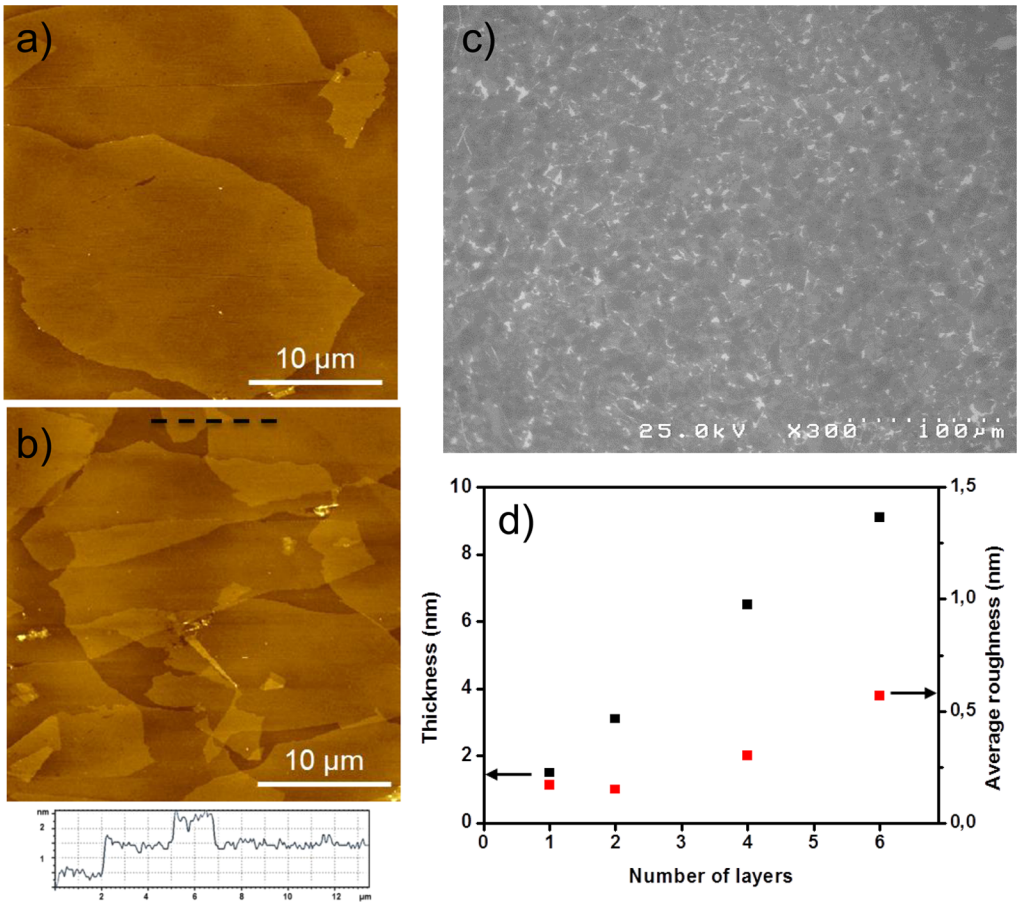

Figure 2. Control of the GO film morphology. (a) AFM images of isolated GO flakes, (b) AFM image at higher coverage obtained by adjustment of the drainage parameters (single deposition step), (c) SEM image of close-packed assembly over a wider area. (d) Thickness and average roughness evolution of as-prepared GO films as a function of the number of deposited layers.

approach lies on the transfer of large GO flakes that remain perfectly flat, even in the case of high-density films. Such a beneficial result comes from the combination of several mechanisms. First, GO sheets at the water/air interface are directly in contact with the substrate during the transfer step. Thus, this approach avoids a commonly encountered problem with alternative solution-based deposition methods: water droplets trapping underneath the sheets, leading to undesired wrinkling after drying.[15] Also, forces induced by capillary interactions and line tension action have an additional effect to stretch the sheets while the retracting aqueous front passes over them.[36]

In addition to the ability of this approach to preserve the flatness of large sheets, Figure 2c also illustrates the remarkable homogeneity of the transferred films over large areas. A layer-by-layer approach then allows precisely adjusting the film thickness while preserving the quality of the film morphology (Figure 2d). Most importantly, in this process of multiple deposition steps, the average roughness (measured on a series of 30 × 30 μm^2 AFM images) remains extremely small. It is, for example, below 0.6 nm for a six-layer thick film, which is more than 3 times lower than literature data for the same thickness.[15]

This hemispherical film-based technique has several advantages such as low volume requirement (<0.5 $\mu L/cm^2$ of deposited film) and high deposition rate, but it is not easily wafer scalable. Indeed, two interdependent limitations have to be faced: (1) it is well-known that, from a limited starting volume of solution, stretching a large bubble cannot result in a dense deposited film;[37] (2) a solution from the latter problem could be an increase of the starting solution concentration but, in the case of GO, this would result in forming a gel-like structure incompatible with the formation of ultrathin films.[38]

2.2. Transfer of Vertical Films. To ensure the scalability of the method, we introduce a new geometry by substituting the hemispherical water−surfactant−GO film with a large and flat vertical one (up to 220 mm in diameter). A free-standing GO stabilized water film is formed by immersing a metallic ring in the GO solution and then by pulling it up vertically. In this position, water starts to drain and the substrate is approached to operate the transfer (Figure 3 a, b). The process ends with a thorough drying and rinsing step. As for the hemispherical film case, the film thickness can be controlled by adjusting the solution concentration, drainage time, and number of depositions. To illustrate the homogeneity of the method, Figure 3 c, d presents scanning electron microscopy (SEM) images and Raman spectra obtained after a single deposition on a 2 in. silicon wafer. After deposition of the GO flakes, the wafer was annealed in vacuum at 350 °C to form an rGO film. We acquired 25 large-area (1500 × 1160 μm^2) SEM images at the locations labeled (1,1) to (5,5) in Figure 3d. They are all reported in Figure S3. Figure 3c presents four of these SEM images along the vertical axis of the wafer showing a uniform high coverage. We also performed Raman spectroscopy at the 17 locations corresponding to red dots in Figure 3d. Four as-measured spectra along a vertical axis of the wafer are displayed in Figure 3d. The 17 spectra are reported in Figure S4. All

DOI: 10.1021/acsami.5b05540
ACS Appl. Mater. Interfaces 2015, 7, 21270−21277

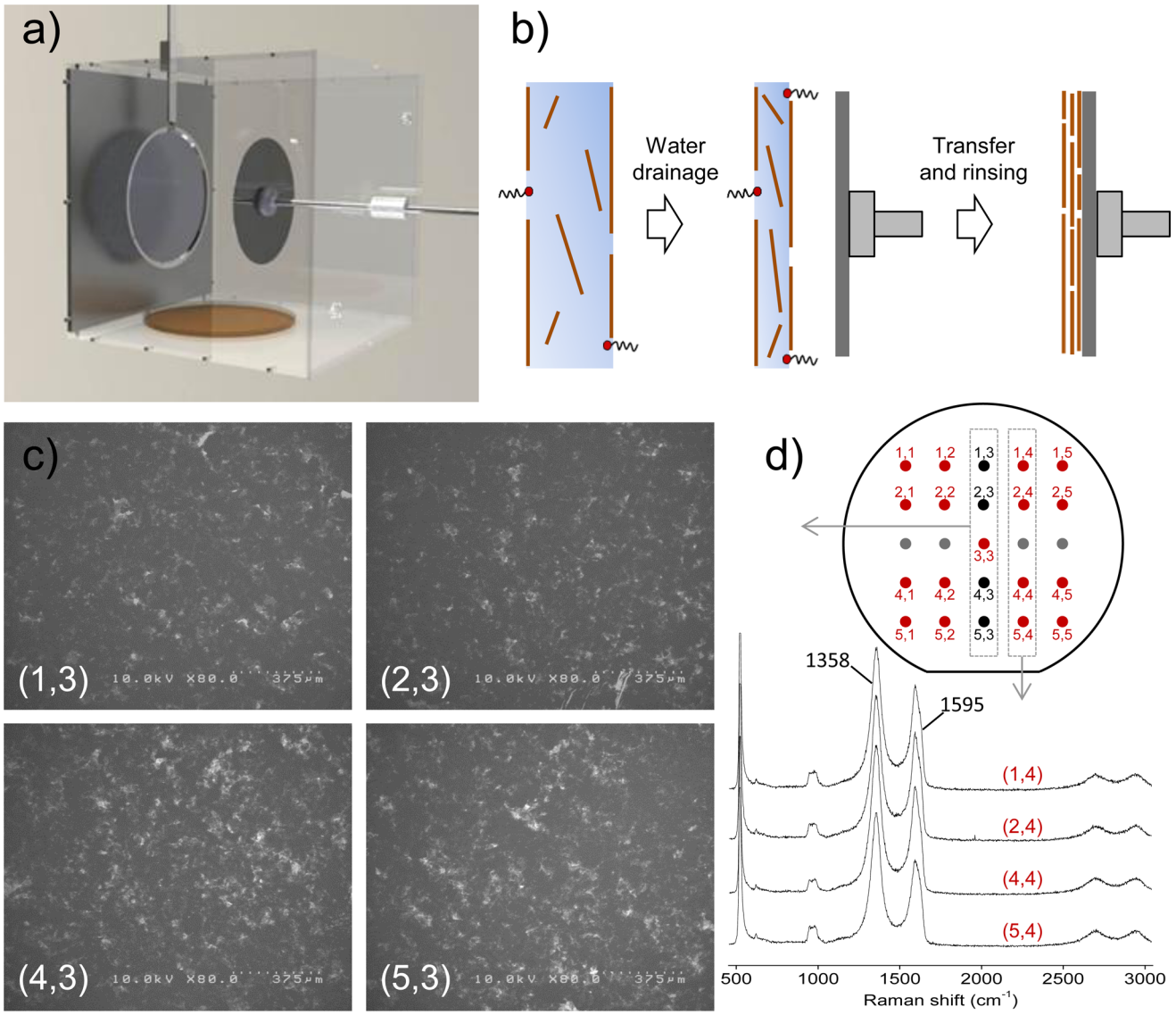

Figure 3. Scalable approach with large vertical surfactant films. (a) Principle of vertical film transfer with a metal ring of 220 mm in diameter. (b) Schematic representation of the process steps leading to GO film formation. (c) SEM images at 4 of the 25 positions. See Figure S3 for all the images. (d) Four of the 17 Raman spectra obtained at the red dot positions. See Figure S4 for all the spectra. Laser wavelength = 532 nm.

intensities of the G band at 1595 cm^{-1} are within ±20% of the mean value with no special evolution with respect to the position over the wafer.

The homogeneity of the method was also confirmed in a complementary experiment in which GO films were assembled on 2 in. quartz wafers and then were converted in rGO. Optical transmittance measurements were performed at 12 different positions separated by 12 mm yield similar values (typically 96% ± 0.5% in the conditions described below). For multiple successive depositions, we found it beneficial to rotate the substrate between each deposition and to avoid transferring the very bottom part of the vertical film.

2.3. Generic Character of the Assembly Technique. The scalability of this approach is not limited to 2 in. wafers. Indeed, we already validated the deposition at the 8 in. (200 mm) wafer scale proving that substrate size is not an issue since the only limitation comes from the dimension of the surfactant film whose stability can be adjusted by changing the surfactant parameters (nature and concentration).

Besides its simplicity and scalability, the method also offers several other important advantages. In particular, whatever the film size, all the drained solution from the film comes back to the starting volume and is then again available to form a second surfactant film with no loss of nano-objects. All the engaged GO flakes are either transferred or reusable. Furthermore, this method can be readily adapted to other types of substrates, in particular flexible and transparent organic substrates. As an example, Figure 4a displays an example of GO flakes transferred on a polyimide substrate. We also recently proved the efficiency of the method by further studying the local reduction of GO films and the conductivity of individual GO flakes in scanning electrochemical microscopy (SECM) studies for which homogeneity and very low rugosity were decisive assets.[39,40]

2.4. Reduction of GO Films and Transparent Electrodes. Having established the potential of the method for the formation of large films, we now turn to its evaluation in the context of transparent electrodes which requires a fine control of the film thickness and a high degree of homogeneity. To convert the insulating GO films into conductive rGO, several

DOI: 10.1021/acsami.5b05540
ACS Appl. Mater. Interfaces 2015, 7, 21270−21277

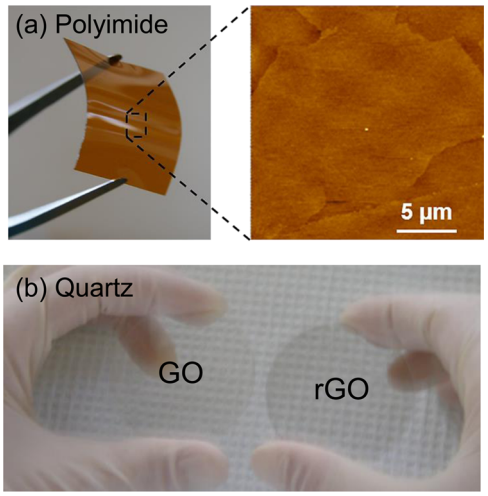

Figure 4. (a) Photograph and AFM image of GO flakes transferred on a polyimide substrate. (b) Thin film of GO (left) and rGO (right) on 2 in. quartz wafers. See text for the reduction method.

reductions are traditionally performed by chemical reductions, thermal annealing, and healing of the GO structure.[38,41−43] In our case, the prepared GO films are first chemically reduced using a combination of hydroiodic (HI) and acetic acids at moderate temperature (40 °C), a method that was demonstrated by Moon et al. to be efficient for both thin and thick GO films.[43] As shown in Figure 4b, this step leads to an evolution of the optical transmittance from quasi-transparent to slightly darker films (from 97.5% to 96% for the film reported in Figure 4b) because of a considerable decrease of various oxygen species as identified by the detailed X-ray photoelectron spectroscopy (XPS) analysis of the carbon 1s core level (C_{1s}) reported in Figure 5. The deconvolution and the assignment of the C_{1s} components in GO and rGO is still a subject of debate in the literature.[44,45] Figure 5 shows that the most significant changes in the C_{1s} XPS spectra occur at the first reduction step. In particular, the HI vapor treatment alone leads to an important decrease of the peak at ca. 287.2 eV associated with epoxide and ether groups and of the peak at ca. 285 eV associated with hydroxyl groups. Simultaneously, this first reduction step leads to the development of a thin and intense peak at ca. 284.1 eV associated with the restoration of sp^2 carbon atoms. The evolution of the spectra after the next reduction steps is less spectacular and is characterized by a continuous decrease of all the contributions from oxygenated carbon except for the COH one which remains rather strong even after annealing at 1000 °C in the presence of acetylene. The sp^2 carbon peak which accounts for 65% of the surface of the spectra after the HI steps increases to 72% in the final spectra showing that further improvement of the graphitization is possible.

The restoration of the sp^2 carbon framework in the first step is associated with an amelioration of the electrical conductivity. However, the most significant improvement of the rGO conductivity is observed after annealing above 600 °C. At this temperature, most of the labile oxygenated species has been already removed, and the improvement of the conductivity is likely because of the partial reconstruction of graphene-like domains creating conductive pathways.[46]

This HI-based chemical vapor prereduction confirms its beneficial effect as it solves the common problem of film delamination[20] while it considerably enhances the film electrical

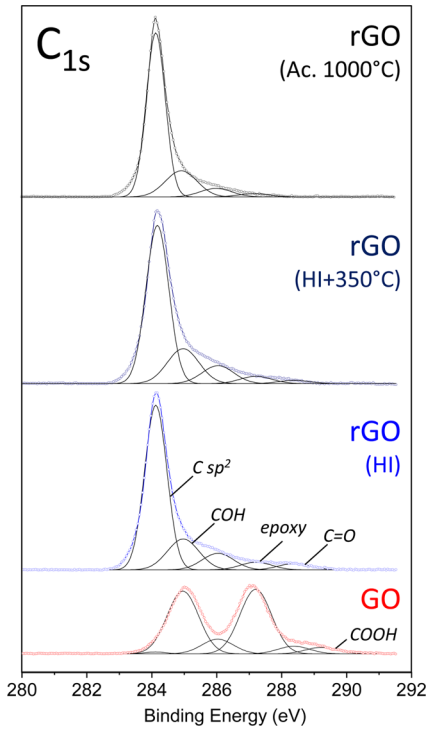

Figure 5. XPS C_{1s} core level spectra of GO and rGO and associated deconvolution. The main components correspond to the sp^2 carbon areas (C═C/C−C) and from hydroxyl, epoxy (C−O/C−O-C), carbonyl (C═O), and carboxyl groups (−COO) formed during the oxidation of graphite by the modified Hummer's method.

property after thermal annealing compared to films not chemically reduced. The prereduction by HI notably improves the conductivity by a factor 4.7 after annealing at 350 °C when compared with annealed-only films (see Figure 6a). One explanation for the benefits of the chemical prereduction before heating GO films lies on the probable conversion of epoxy groups into hydroxyls groups which are removed at lower temperatures. The conversion and the elimination introduce less disorder in the carbon lattice by preventing the creation of carbon vacancies (by decreasing CO and CO_2 releases) and the formation of stable oxygen arrangements (carbonyls, ether rings, etc.) which would definitively trap oxygen atoms in the carbon lattice during high-temperature annealing.[17] A further significant step is made by annealing the chemically reduced GO films in the presence of acetylene. Above 800 °C, a considerable enhancement of the rGO film conductivity is observed while the obtained transmittance is totally in accordance with the expected one. For example, as shown in Figure 6b, a transmittance of 94.8% is obtained for a two-layer rGO film which fits the expected loss of 2.3% transparency by graphene layer. Importantly, this accuracy also indicates that, with these parameters, there is no undesirable carbon deposition.[42]

The recovery of large sp^2 domains and their associated electrical properties opens the possibility to integrate these rGO films in a broad range of applications requiring transparent electrodes. Figure 6c displays a comparison between the performances of our rGO films (after acetylene healing) with literature data. While this method is particularly well-suited for the realization of electrodes in the high-transparency range (>90%), the conductivities of the prepared electrodes are among the highest reported for rGO films (before any

DOI: 10.1021/acsami.5b05540
ACS Appl. Mater. Interfaces 2015, 7, 21270−21277

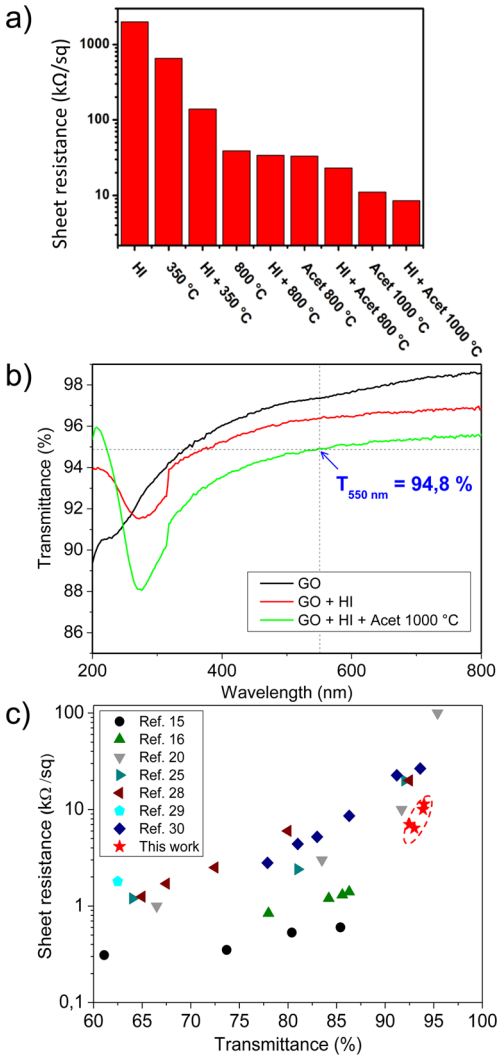

Figure 6. Reduced graphene oxide based electrodes. (a) Films deposited on 2 in. quartz substrates before and after chemical reduction. (b) Evolution of a two-layer film transmittance after chemical reduction and healing step. (c) Sheet resistance of the prepared electrodes under acetylene atmosphere (1000 °C) versus transmittances (measured at 550 nm) compared with rGO literature data.

additional doping procedure).[3] For instance, an electrode composed of three layers of rGO shows a transmittance as high as 93% and a resistance as low as 6.4 kohm/sq confirming both the high quality of the layer stacking and the efficiency of the lattice restoration.

3. EXPERIMENTAL SECTION

3.1. Materials. Chemicals and solvents of research grade were purchased from Sigma-Aldrich and were used as received. Ultrapure water (18.2 MΩ) was produced by a Milli-Q system. Graphite powder was purchased from Sinocarbon Material technology Co.

3.2. Preparation of GO Solutions. Graphene oxide solutions are obtained by a modified chemical exfoliation method described elsewhere.[16] Briefly, 0.5 g of graphite, 25 mL of concentrated H_2SO_4, and 2 g of $NaNO_3$ were mixed at 0 °C. While keeping the mixture stirring at 0 °C, 3 g of $KMnO_4$ was added in small portions. At the end of this stage, the mixture was kept on stirring for 90 min at 0 °C and then for 2 h at 35 °C. Fifty milliliters of distilled water was then slowly added and the solution was stirred for additional 30 min. Next, 2.5 mL of H_2O_2 (30%) was dropped, and the stirring was continued for 15 min. The mixture was then mainly composed of graphite oxide. It was then separated in 25 mL tubes which went through five successive steps of (1) centrifugation at 1600 rpm, (2) elimination of 20 mL supernatant, (3) addition of 20 mL distilled water, (4) agitation with a laboratory vortex shaker enabling exfoliation of GO (the last agitation step led to the formation of a gel-like structure composed of large GO flakes with remaining unexfoliated graphite oxide), and (5) low speed centrifugation to separate GO from graphite oxide. After the separation process, a solution of graphene oxide at ca. 4 mg mL^{-1} was obtained. For the hemispherical water film template, the solution used was composed of 1.3 mg mL^{-1} GO and 0.5 CMC (critical micellar concentration) of sodium dodecylbenzenesulfonate. Larger vertical GO stabilized water films required a small increase of the surfactant concentration to 1 CMC for a 2 in. and 2 CMC for a 4 in. deposited film while keeping the GO concentration at 0.73 mg mL^{-1}. Using a different GO oxidation/exfoliation procedure or a different GO concentration would require reoptimizing the deposition parameters. This can be simply done by first measuring the stability time of the water film and then testing a few depositions at different drainage durations to establish the draining-time/deposited-density relation which is then very stable.

3.3. Formation of GO Films. Before deposition, the silicon or quartz substrates are degreased with acetone and ethanol and are cleaned in a mixture of concentrated nitric and hydrochloric acid (1:3) at 90 °C for 1 h. The deposition chamber and metallic ring (in the vertical film case) are also regularly cleaned. For the hemispherical water film method, a bubble is first prepared at the tip of a Pasteur pipet and is gently deposited at the bottom of the glass chamber which also contains water to increase the humidity level (which helps stabilizing the water film). The chamber is closed by a cap through which a mobile rod allows moving the sample toward the bubble. A schematic is provided in the Supporting Information. For the vertical film geometry, a beaker of water (to increase humidity level) and a beaker containing the GO-solution are inserted in the chamber. The metallic ring is placed horizontally into the solution and is slowly moved back to its vertical position avoiding vibrations. Several tests of water film stability are done until no spontaneous film bursting occurs before 30 s. The wafer is then moved in contact with the film after a controlled drainage time of typically 10 s adjusted upon the targeted film morphology. As gravity induces an increased thickness and increased GO concentration at the very bottom of the ring, this area is avoided.

After each GO deposition, surfactant molecules are removed using the following protocol: (1) the sample is dried at 50 °C on a hot plate for 15 min, (2) an initial rinsing step is performed using a few water droplets gently deposited on the surface to avoid flake removal, (3) thorough rinsing is performed using water and then ethanol, and (4) the sample is finally dried again at 50 °C on a hot plate.

3.4. Reduction Methods. GO-coated quartz or silicon substrates were placed in an isolated jar containing a mixture of HI and acetic acid (2:5) and were heated at 40 °C for 24 h.[38] To remove the HI/acetic acid mixture with no alteration of the film, the samples were transferred to a second closed jar containing ethanol heated at 40 °C for 3 h. For thermal

DOI: 10.1021/acsami.5b05540
ACS Appl. Mater. Interfaces 2015, 7, 21270−21277

annealing, the substrates were placed in a traditional tube oven and were heated at a rate of 4 °C min^{-1} in a 10^{-6} mbar vacuum and were maintained at the desired temperature for 1 h. Acetylene annealing was carried out by placing the samples in a quartz tube filled with argon (1 L/min). At the desired temperature (800 or 1000 °C), 0.3 and 0.02 L min^{-1} of H_2 (to prevent amorphous carbon deposition) and C_2H_2, respectively, were introduced during 5 min.

3.5. Characterizations. Optical transmittances of the GO films were measured using a UV−vis spectrophotometer (Lambda 900, PERKIN ELMER). Raman spectra were performed on a HORIBA Jobin Yvon LabRAM ARAMIS spectrometer with excitation wavelength of 532 nm and laser power of 100 μW. Sheet resistances were measured from a standard four probe station (JANDEL Multiheight probe). The film morphologies were analyzed by tapping mode (Si tip) atomic force microscopy (AFM 5500 LS, Agilent Technologies) and with the PicoImage software. SEM images were performed using a Hitachi S4500 microscope. The XPS system is a KRATOS Axis Ultra DLD with a monochromated Al Kα line operating at 1486.6 eV. The vacuum in the sample chamber was 5×10^{-9} Torr. The spectrometer was calibrated by assuming the binding energy of the Au 4f 7/2 line at 84 eV with respect to the Fermi level.

4. CONCLUSION

In summary, an inexpensive, substrate-independent, and scalable technique was developed for the formation of large GO films with unprecedented smoothness. The precise control over the number of deposited layers enables the preparation of transparent electrodes with tuned transparencies and conductivities. By the combination of this deposition method with reduction under acetylene atmosphere, the performances of the as-prepared rGO electrodes are among the best reported to date. Thus, this approach represents a new step toward the scalability of graphene oxide liquid phase processing and could be used in a variety of applications ranging from GO coatings to rGO-based large-scale/low-cost electronics.

■ ASSOCIATED CONTENT

Supporting Information

The Supporting Information is available free of charge on the ACS Publications website at DOI: 10.1021/acsami.5b05540.

Additional transfer protocol schematic (Figure S1), AFM images before surfactant rinsing (Figure S2), SEM images (Figure S3), and Raman spectra (Figure S4) (PDF)

■ AUTHOR INFORMATION

Corresponding Authors

*E-mail: stephane.campidelli@cea.fr.
*E-mail: vincent.derycke@cea.fr.

Notes

The authors declare no competing financial interest.

■ ACKNOWLEDGMENTS

The authors thank Pascal Senat and Dominique Duet for technical support, Romain Bourrellier and Jinbo Bai for experimental help, and Jocelyne Leroy for XPS analysis. This work was principally supported by the Direction Générale de l'Armement (DGA) through the contract N°REI 2009.34.0011.00000000. It was also partially supported by a public grant overseen by the French National Research Agency (ANR) as part of the "Investissements d'Avenir" program (Labex NanoSaclay, reference: ANR-10-LABX-0035), project Figaro.

■ REFERENCES

(1) Geim, A. K.; Novoselov, K. S. The Rise of Graphene. *Nat. Mater.* **2007**, *6*, 183−191.
(2) Wan, X.; Huang, Y.; Chen, Y. Focusing on Energy and Optoelectronic Applications: a Journey for Graphene and Graphene Oxide at Large Scale. *Acc. Chem. Res.* **2012**, *45*, 598−607.
(3) Huang, X.; Zeng, Z.; Fan, Z.; Liu, J.; Zhang, H. Graphene-Based Electrodes. *Adv. Mater.* **2012**, *24*, 5979−6004.
(4) Bae, S.; Kim, H.; Lee, Y.; Xu, X.; Park, J.-S.; Zheng, Y.; Balakrishnan, J.; Lei, T.; Kim, H. R.; Song, Y. I.; Kim, Y.-J.; Kim, K. S.; Özyilmaz, B.; Ahn, J.-H.; Hong, B. H.; Iijima, S. Roll-to-Roll Production of 30-in. Graphene Films for Transparent Electrodes. *Nat. Nanotechnol.* **2010**, *5*, 574−578.
(5) Wu, Y.; Lin, Y.; Bol, A. A.; Jenkins, K. A.; Fengnian Xia, F.; Farmer, D. B.; Zhu, Y.; Avouris, P. High-Frequency, Scaled Graphene Transistors on Diamond-like Carbon. *Nature* **2011**, *472*, 74−78.
(6) Wu, Y.; Jenkins, K. A.; Valdes-Garcia, A.; Farmer, D. B.; Zhu, Y.; Bol, A. A.; Dimitrakopoulos, C.; Zhu, W.; Xia, F.; Avouris, P.; Lin, Y.-M. State-of-the-Art Graphene High-Frequency Electronics. *Nano Lett.* **2012**, *12*, 3062−3067.
(7) Green, A. A.; Hersam, M. C. Solution Phase Production of Graphene with Controlled Thickness via Density Differentiation. *Nano Lett.* **2009**, *9*, 4031−4036.
(8) Lotya, M.; Hernandez, Y.; King, P. J.; Smith, R. J.; Nicolosi, V.; Karlsson, L. S.; Blighe, F. M.; De, S.; Wang, Z.; McGovern, I. T.; Duesberg, G. S.; Coleman, J. N. Liquid Phase Production of Graphene by Exfoliation of Graphite in Surfactant/Water Solutions. *J. Am. Chem. Soc.* **2009**, *131*, 3611−3620.
(9) Hernandez, Y.; Nicolosi, V.; Lotya, M.; Blighe, F. M.; Sun, Z.; De, S.; McGovern, I. T.; Holland, B.; Byrne, M.; Gun'Ko, Y. K.; Boland, J. J.; Niraj, P.; Duesberg, G.; Krishnamurthy, S.; Goodhue, R.; Hutchison, J.; Scardaci, V.; Ferrari, A. C.; Coleman, J. N. High-Yield Production of Graphene by Liquid-Phase Exfoliation of Graphite. *Nat. Nanotechnol.* **2008**, *3*, 563−568.
(10) Cui, X.; Zhang, C.; Hao, R.; Hou, Y. Liquid-Phase Exfoliation, Functionalization and Applications of Graphene. *Nanoscale* **2011**, *3*, 2118−2126.
(11) Shih, C.-J.; Vijayaraghavan, A.; Krishnan, R.; Sharma, R.; Han, J.-H.; Ham, M.-H.; Jin, Z.; Lin, S.; Paulus, G. L. C.; Reuel, N. F.; Wang, Q. H.; Blankschtein, D.; Strano, M. S. Bi- and Trilayer Graphene Solutions. *Nat. Nanotechnol.* **2011**, *6*, 439−445.
(12) Paredes, J. I.; Villar-Rodil, S.; Martínez-Alonso, A.; Tascón, J. M. D. Graphene Oxide Dispersions in Organic Solvents. *Langmuir* **2008**, *24*, 10560−10564.
(13) Wang, X.; Bai, H.; Shi, G. Size Fractionation of Graphene Oxide Sheets by pH-Assisted Selective Sedimentation. *J. Am. Chem. Soc.* **2011**, *133*, 6338−6342.
(14) Lin, X.; Shen, X.; Zheng, Q.; Yousefi, N.; Ye, L.; Mai, Y.-W.; Kim, J.-K. Fabrication of Highly-Aligned, Conductive, and Strong Graphene Papers Using Ultralarge Graphene Oxide Sheets. *ACS Nano* **2012**, *6*, 10708−10719.
(15) Zheng, Q.; Ip, W. H.; Lin, X.; Yousefi, N.; Yeung, K. K.; Li, Z.; Kim, J.-K. Transparent Conductive Films Consisting of Ultralarge Graphene Sheets Produced by Langmuir−Blodgett Assembly. *ACS Nano* **2011**, *5*, 6039−6051.
(16) Zhao, J.; Pei, S.; Ren, W.; Gao, L.; Cheng, H.-M. Efficient Preparation of Large-Area Graphene Oxide Sheets for Transparent Conductive Films. *ACS Nano* **2010**, *4*, 5245−5252.
(17) Bagri, A.; Mattevi, C.; Acik, M.; Chabal, Y. J.; Chhowalla, M.; Shenoy, V. B. Structural Evolution During the Reduction of Chemically Derived Graphene Oxide. *Nat. Chem.* **2010**, *2*, 581−587.
(18) Zheng, Q.; Li, Z.; Yang, J.; Kim, J.-K. Graphene Oxide-Based Transparent Conductive Films. *Prog. Mater. Sci.* **2014**, *64*, 200−247.

DOI: 10.1021/acsami.5b05540
ACS Appl. Mater. Interfaces 2015, 7, 21270−21277

(19) He, Q.; Sudibya, H. G.; Yin, Z.; Wu, S.; Li, H.; Boey, F.; Huang, W.; Chen, P.; Zhang, H. Centimeter-Long and Large-Scale Micropatterns of Reduced Graphene Oxide Films: Fabrication and Sensing Applications. *ACS Nano* **2010**, *4*, 3201−3208.
(20) Becerril, H. A.; Mao, J.; Liu, Z.; Stoltenberg, R. M.; Bao, Z.; Chen, Y. Evaluation of Solution-Processed Reduced Graphene Oxide Films as Transparent Conductors. *ACS Nano* **2008**, *2*, 463−470.
(21) Cote, L. J.; Kim, F.; Huang, J. Langmuir−Blodgett Assembly of Graphite Oxide Single Layers. *J. Am. Chem. Soc.* **2009**, *131*, 1043−1049.
(22) Chen, C.; Yang, Q.-H.; Yang, Y.; Lv, W.; Wen, Y.; Hou, P.-X.; Wang, M.; Cheng, H.-M. Self-Assembled Free-Standing Graphite Oxide Membrane. *Adv. Mater.* **2009**, *21*, 3007−3011.
(23) Azevedo, J.; Costa-Coquelard, C.; Jegou, P.; Yu, T.; Benattar, J.-J. Highly Ordered Monolayer, Multilayer, and Hybrid Films of Graphene Oxide Obtained by the Bubble Deposition Method. *J. Phys. Chem. C* **2011**, *115*, 14678−14681.
(24) Dikin, D. A.; Stankovich, S.; Zimney, E. J.; Piner, R. D.; Dommett, G. H. B.; Evmenenko, G.; Nguyen, S. T.; Ruoff, R. S. Preparation and Characterization of Graphene Oxide Paper. *Nature* **2007**, *448*, 457−460.
(25) Yamaguchi, H.; Eda, G.; Mattevi, C.; Kim, H.; Chhowalla, M. Highly Uniform 300 mm Wafer-Scale Deposition of Single and Multilayered Chemically Derived Graphene Thin Films. *ACS Nano* **2010**, *4*, 524−528.
(26) Lv, W.; Xia, Z.; Wu, S.; Tao, Y.; Jin, F.-M.; Li, B.; Du, H.; Zhu, Z.-P.; Yang, Q.-H.; Kang, F. Conductive Graphene-Based Macroscopic Membrane Self-Assembled at a Liquid−Air Interface. *J. Mater. Chem.* **2011**, *21*, 3359−3364.
(27) Chen, W.; Yan, L. Centimeter-Sized Dried Foam Films of Graphene: Preparation, Mechanical and Electronic Properties. *Adv. Mater.* **2012**, *24*, 6229−6233.
(28) Wang, J.; Liang, M.; Fang, Y.; Qiu, T.; Zhang, J.; Zhi, L. Rod-Coating: Towards Large-Area Fabrication of Uniform Reduced Graphene Oxide Films for Flexible Touch Screens. *Adv. Mater.* **2012**, *24*, 2874−2878.
(29) Wang, X.; Zhi, L.; Müllen, K. Transparent, Conductive Graphene Electrodes for Dye-Sensitized Solar Cells. *Nano Lett.* **2008**, *8*, 323−327.
(30) Shin, H.-J.; Kim, K. K.; Benayad, A.; Yoon, S.-M.; Park, H. K.; Jung, I.-S.; Jin, M. H.; Jeong, H.-K.; Kim, J. M.; Choi, J.-Y.; Lee, Y. H. Efficient Reduction of Graphite Oxide by Sodium Borohydride and Its Effect on Electrical Conductance. *Adv. Funct. Mater.* **2009**, *19*, 1987−1992.
(31) Costa-Coquelard, C.; Jegou, P.; Benattar, J.-J. Role of Substrate Wettability in the "Bubble Deposition Method" Applied to the $CeVO_4$ Nanowire Films. *Langmuir* **2011**, *27*, 4397−4402.
(32) Petkova, R.; Benattar, J.-J.; Zoonens, M.; Zito, F.; Popot, J.-L.; Polidori, A.; Jasseron, S.; Pucci, B. Free-Standing Films of Fluorinated Surfactants as 2D Matrices for Organizing Detergent-Solubilized Membrane Proteins. *Langmuir* **2007**, *23*, 4303−4309.
(33) Tang, G.; Zhang, X.; Yang, S.; Derycke, V.; Benattar, J.-J. New Confinement Method for the Formation of Highly Aligned and Densely Packed Single-Walled Carbon Nanotube Monolayers. *Small* **2010**, *6*, 1488−1491.
(34) Kim, J.; Cote, L. J.; Kim, F.; Yuan, W.; Shull, K. R.; Huang, J. Graphene Oxide Sheets at Interfaces. *J. Am. Chem. Soc.* **2010**, *132*, 8180−8186.
(35) Kim, F.; Cote, L. J.; Huang, J. Graphene Oxide: Surface Activity and Two-Dimensional Assembly. *Adv. Mater.* **2010**, *22*, 1954−1958.
(36) Costa-Coquelard, C.; Azevedo, J.; Ardiaca, F.; Benattar, J.-J. Spontaneous and Dense Assemblies of Nanoparticles within Micro-Channels by the Bubble Deposition Method. *Appl. Surf. Sci.* **2013**, *264*, 364−367.
(37) Yu, G.; Cao, A.; Lieber, C. M. Large-Area Blown Bubble Films of Aligned Nanowires and Carbon Nanotubes. *Nat. Nanotechnol.* **2007**, *2*, 372−377.
(38) Xu, Z.; Gao, C. Graphene Chiral Liquid Crystals and Macroscopic Assembled Fibres. *Nat. Commun.* **2011**, *2*, 571.
(39) Azevedo, J.; Fillaud, L.; Bourdillon, C.; Noel, J.-M.; Kanoufi, F.; Jousselme, B.; Derycke, V.; Campidelli, S.; Cornut, R. Localized Reduction of Graphene Oxide by Electrogenerated Naphthalene Radical Anions and Subsequent Diazonium Electrografting. *J. Am. Chem. Soc.* **2014**, *136*, 4833−4836.
(40) Bourgeteau, T.; Le Vot, S.; Bertucchi, M.; Derycke, V.; Campidelli, S.; Cornut, R.; Jousselme, B. New Insights into the Electronic Transport of Reduced Graphene Oxide Using Scanning Electrochemical Microscopy. *J. Phys. Chem. Lett.* **2014**, *5*, 4162−4166.
(41) Mao, S.; Pu, H.; Chen, J. Graphene Oxide and its Reduction: Modeling and Experimental Progress. *RSC Adv.* **2012**, *2*, 2643−2662.
(42) Liang, Y.; Frisch, J.; Zhi, L.; Norouzi-Arasi, H.; Feng, X.; Rabe, J. P.; Koch, N.; Müllen, K. Transparent, Highly Conductive Graphene Electrodes from Acetylene-Assisted Thermolysis of Graphite Oxide Sheets and Nanographene Molecules. *Nanotechnology* **2009**, *20*, 434007−434012.
(43) Moon, I. K.; Lee, J.; Ruoff, R. S.; Lee, H. Reduced Graphene Oxide by Chemical Graphitization. *Nat. Commun.* **2010**, *1*, 73.
(44) Dreyer, D. R.; Park, S.; Bielawski, C. W.; Ruoff, R. S. The Chemistry of Graphene Oxide. *Chem. Soc. Rev.* **2010**, *39*, 228−240.
(45) Lim, S. P.; Pandikumar, A.; Lim, Y. S.; Huang, N. M.; Lim, H. N. In-situ Electrochemically Deposited Polypyrrole Nanoparticles Incorporated Reduced Graphene Oxide as an Efficient Counter Electrode for Platinum-Free Dye-Sensitized Solar Cells. *Sci. Rep.* **2014**, *4*, 1−7.
(46) Mattevi, C.; Eda, G.; Agnoli, S.; Miller, S.; Mkhoyan, K. A.; Celik, O.; Mastrogiovanni, D.; Granozzi, G.; Garfunkel, E.; Chhowalla, M. Evolution of Electrical, Chemical, and Structural Properties of Transparent and Conducting Chemically Derived Graphene Thin Films. *Adv. Funct. Mater.* **2009**, *19*, 2577−2583.

DOI: 10.1021/acsami.5b05540
ACS Appl. Mater. Interfaces 2015, 7, 21270−21277